Int. J. Electrochem. Sci., 14 **(2019)** 10469 – 10489, doi: 10.20964/2019.11.54

International Journal of
ELECTROCHEMICAL
SCIENCE
www.electrochemsci.org

Performance and Aging Study of a Proton Exchange Membrane with Different Materials at Different Temperatures and Humidities

Bai Qiang[1], *Li Shaobo*[1,*], *Chuang-Yu Hsieh*[2], *Fang-Bor Weng*[3], *Hsiou-Ming Ou*[3]

[1] College of Mechanical Engineering, Guizhou University, Guiyang 550000, P R China;
[2] Department of Automotive Engineering, Tsinghua University, Beijing 100084, P R China;
[3] Department of Mechanical Engineering & Fuel Cell Center, Yuan Ze University, Taoyuan 320, Taiwan
[*]E-mail: lishaobo@gzu.edu.cn

Received: 29 May 2019 / *Accepted:* 10 September 2019 / *Published:* 7 October 2019

By changing the material for a membrane electrode assembly (MEA) of a fuel cell and controlling the mode of gas inflow, along with the working temperature and humidity, the performance change of the fuel cell and the aging of the MEA under low humidity were studied. It was found that with the decrease of humidity from 100% RH to 50% RH, the decline of cell performance ranged from 8.4% to 64%. Due to the hydrophilicity of silicon dioxide (SiO_2), the addition of SiO_2 into the MEA helped the membrane have better water retention; the current density greatly increased with a decline of cell performance that ranged from 17% to 44% at 50% RH. After the area of the MEA was increased, it was found that with a decrease of relative humidity, the performance decreased by 21% - 36%. Under 100% RH and after a 100-h cyclic dynamic load aging test, the performance decline of fuel cells was 27.2% and the performance decline of the ECSA was 33.3%. Under 50% RH, the performance decrease was 51.8% and the ECSA decrease was 55.3%. The impedance increase and the fluctuating decrease of the OCV of fuel cells under 100% RH were obviously less than those under 50% RH.

Keywords: Humidity; Silicon Dioxide; Membrane Aging; Performance Decline

1. INTRODUCTION

A proton exchange membrane fuel cell (PEMFC) has characteristics of low pollution, high energy conversion efficiency (approximately 40-60%), near normal temperature operation (40-100℃) and fast start-up [1-3]; thus, it is suitable for transportation, portable power and household generators. However, there are several problems in the commercial use of fuel cells, one of which is water management, which will affect the performance and life of the cells [4-6]. At present, one of the

development directions of automotive and portable fuel cells is operating at high temperature and low humidity. In this environment, a lack of water in the MEA will lead to insufficient hydrogen ion conduction, which will decrease the performance of the cells. Currently, the research of MEA with high temperature and low humidity is mainly divided into the following aspects: hydrophilic or hydrophobic materials are added to the gas diffusion layer and the catalytic layer to improve the performance of fuel cells in a high-temperature and low-humidity environment [7-11]; a MEA is prepared by a new technology, and the operation of PEMFC under conditions of low or no humidity are studied [12]; a change of the catalyst content in the MEA catalyst layer or the use of a new catalyst material to explore the change of cell performance in a high-temperature and low-humidity environment [11-13]; or a theoretical model of PEMFCs is established to analyze the water balance in the working process, and the performance of the cells is improved by optimizing the parameters [14-15]. In addition, long-term operation of the cells in a high-temperature and low-humidity environment accelerates the aging and performance decline of MEA. Therefore, research on the causes of membrane aging is also a hot topic in research. Researchers from several groups found that the dissolution and aggregation of Pt catalysts were the main reasons for the performance decline of cells [16-20]. At the same time, it was found that the corrosion of the carbon plate also led to a performance decline of the cells [20]. Another important research direction is to improve the performance of cells or delay the performance decline by changing the material of the catalyst or carbon plate [20-25]. It was found that the performance decline of cells and the aging of MEA are quite different under different working conditions (such as acidic, alkaline or with strongly oxidizing working conditions) or different working modes (such as frequent stop-start, long-time full-load or low-load operations) [26-28]. Wang Likun and coworkers [29,30] found that the technology of a nanoplatelet alloy/Nafion catalytic interface and gold nanoparticle/titania ultrathin film heterogeneous catalysts can improve the PEMFC performance in hydrogen containing a small amount of monoxide. This research will greatly promote the commercialization of PEMFCs and reduce the cost of hydrogen.

In this paper, a Pt CCM (catalyst-coated membrane, a slow spraying process in which a catalyst solution is sprayed directly on an MEA to overcome the wet expansion problem of the MEA) is applied on an MEA; the content of the Pt catalyst at the anode and cathode is 0.2 mg/cm^2 and 0.4 mg/cm^2, respectively. The changes in cell performance at different operating temperatures, gas flow rates and levels of relative humidity are studied. Based on the water retention of SiO_2 [8, 9], the performance change of the cell under high temperature and low humidity is investigated by adding SiO_2 to the catalyst layer. The changes to the electrochemically active surface area (ECSA), AC impedance and open-circuit voltage (OCV) of the cell under different levels of humidity are studied by dynamic load during long-term cycling, and the deep-seated causes of aging and decline of cell performance are further analyzed.

2. EXPERIMENTAL

2.1. Preparation of a fuel cell membrane

The membrane was made by CCM technology in a laboratory. CCMs can be divided into two methods, with one being decal transfer (Decal-CCM), which sprays the catalyst solution onto the

transfer substrate and then transfers the catalyst layer to both sides of a membrane by hot pressing. The substrate used in this method was smoother than a GDL, so the interface impedance could be reduced. Decal-CCM cannot accurately control the catalyst load on the artificial operation, and it is easy to cause MEA performance instability due to uneven coating. Another method is direct spraying, direct spraying combined with ultrasonic oscillator in spraying process can greatly improve the uniformity of MEA spraying and precisely control the amount of catalyst to ensure the stability of MEA performance. In summary, the direct spraying method was used as the preparation method of MEA.

Catalysts were sprayed onto the membrane by an automatic spraying machine (Sono-Tek, US), and the electrolyte membrane was Nafion®-HP (DuPont Co. US). First, the catalyst (Johnson Matthey, HiSPEC 4310, UK) was mixed with a 5 wt% Nafion solution (DuPont Co., USA), and then isopropanol solvent (Jingming Chemical Company of China) and deionized water were added. The content ratio of catalyst to Nafion was 2:1, and the solution was placed in an ultrasonic oscillator for two hours to make the solution evenly distributed. Second, isopropanol was used to clean the spraying pipeline of the automatic spraying machine. The air bottle was opened, and the temperature of the heating plate was set to 90℃. Third, when the temperature of the heating plate reached 90℃, the solution was placed in the automatic spraying machine (Sono-Tek, USA), and the positioning test was done to determine whether the solution could be sprayed. Fourth, the spraying parameters were set, and a test path was run to determine whether the spraying position was correct. After confirming everything was correct, the spraying experiment was carried out. Fifth, after spraying, the MEA was placed in a circulating oven and dried at room temperature for 24 h. Finally, the dried MEA was weighed on a micro balance (Meltler-Toledo Pac Rim AG-XS205, Switzerland), and the spray weight was calculated to ensure that the catalyst content met the experimental requirements.

2.2. Assembly process of a fuel cell

Industrial alcohol (Youhe Trading Company, China) was used to wipe and remove surface stains from a bipolar plate and a graphite plate. An end plate and the bipolar plate were placed together. Eight bolts were inserted into fixed positions in the end plate, and then a Teflon tube was used to cover the bolts to prevent the bolt positions from shaking and the cathode and anode from interfering. The graphite runner plate was placed on the bipolar plate, and an airtight gasket was fixed on the graphite runner plate by a bolt. The MEA was fitted with an airtight gasket and the other half of the cell was gently buckled on the MEA and fixed by a bolt. Finally, the tightening pressure was increased to 25 kgf·cm by a diagonally progressive method with a torque wrench, and the cell was assembled.

2.3. Explanation of fuel cell testing

The first step before cell testing was activation. After activation for 12 hours, the stability and performance of the polarization curve met the requirements, which indicated that the activation was

completed. The performance of the cell was tested by a scanning voltage mode. The ECSA of the fuel cell catalyst was measured by cyclic voltammetry. The formulas are as follows:

$$ECSA = \frac{10000 \times A_d}{c \times m \times v} \quad (1)$$

$$A_d = Q_h = \int_{0.05}^{0.4} (i - i_{DL}) dV \quad (2)$$

For equation (1), the unit of ECSA is m^2/g_{Pt}, A_d is the integral area of the hydrogen adsorption peak (AV), c is the coefficient of hydrogen adsorption of Pt (0.21 mC/cm^2), m is the content of Pt in the cathode (mg), and v is the scanning speed of the cyclic voltammetry (mV/sec). Equation (2) is the integral area of the hydrogen adsorption peak, where i represents the measured current (mA), i_{DL} is the double-layer current (mA), and the integral range is approximately 0.05-0.4 V. Using the change of high and low current as an aging test method for the fuel cell corresponded to the actual working conditions of the cell. The operating voltage that corresponded to the high and low current in this experiment was 0.6-0.8 V. After applying a cyclic dynamic load for a long period, the aging extent of the cell was judged by the performance of the polarization curve, and the aging of the catalyst and MEA was analyzed for electrochemical characteristics to understand the performance of the accelerated aging.

2.4. Experiments on CV and EIS

In this paper, a model 850C fuel cell test platform (Scribner Associates) was used. First, the fuel cell was activated, then the performance polarization curve was drawn, and the AC impedance of the cell was measured. Finally, the electrochemically active surface area (ECSA) of the cell was measured by cyclic voltammetry. The scanning rate of CV curves(0V ~ 1.2V) are 50mV/s. The scanning rate of long time dynamic load is 0.1V/3s, and the voltage rises from 0.6 V ~ 0.8 V as a cycle. The frequency range of EIS is 10KHz~0.1Hz, and a wide range of frequency scanning can more accurately to distinguish the losses caused by various effects.

AC impedance is also called electrochemical impedance spectroscopy (EIS). AC impedance is a measurement method where a small amplitude sinusoidal wave potential (or current) is applied as a disturbance signal. On the one hand, it avoids large changes to the system; on the other hand, it can also make the disturbance impact on the system approximately linear, which simplifies the measurement data processing. EIS was used to diagnose the AC impedance of the cell under different conditions and to estimate the basic characteristics of the membrane impedance, electrode impedance and electrochemical dynamic mechanism. EIS was also used to calculate the influence of various operating conditions on the performance of the cell. The performance loss caused by various effects can also be more accurately distinguished by a wide range of frequency scanning. Cyclic voltammetry can check the ECSA of the catalyst on the electrode. The basic analysis and measurement system was established based on the test platform where the cathode and the anode were respectively fed with hydrogen and air, and a different potential was set for the cell to observe the peak area of hydrogen adsorption.

3. RESULTS AND DISCUSSION

3.1. Effect of different relative humidity and gas supply on cell performance

Through relevant papers [31, 32, 33, 34, 35, 36, 37, 38, 39] and previous experiments, it was found that the working voltage of commercial fuel cells was generally between 0.6-0.8 V; within this range, the cells achieved relatively stable maximum power and performance. Based on this, the current density at 0.6 V was used as the standard of cell performance. To simulate real working situations, a cyclic voltage of 0.6 V-0.8 V was used as the working mode for a long-term dynamic load experiment to detect the aging condition of fuel cell performance.

3.1.1 Performance comparison at 65℃ [40]

Gas supply for fuel cells can be divided into two types: flow rate and fixed stoichiometry. Figure 1a and c shows the polarization and impedance curves of a cell under different levels of humidity with a fixed flow rate (150 ml/min for the anode and 250 ml/min for the cathode). Under 100% RH and 0.6 V, the cell performance was 473.5 mA/cm^2; under 50% RH and 0.6 V the performance was 205.8 mA/cm^2, which was a decrease of 57%. Figure 1c shows that the ohmic impedance and polarization impedance of the cell increase rapidly with the decrease of relative humidity. Figure 1b and d is the polarization curve and AC impedance curve of the cell under different relative humidity with a fixed stoichiometry (anode: 1.2 times/cathode: 4 times). The cell's performance was 559.12 mA/cm^2 at 100% RH and 0.6 V and 512.02 mA/cm^2 at 50% RH. The performance of the cell did not decline significantly, which indicated that the Nafion®-HP had a more stable performance when the gas supply was at a fixed stoichiometry. It can be seen from the impedance curve that with the decrease of relative humidity, the impedance of the cell hardly changed in the early stage, but then increased rapidly. With the decrease of humidity, the MEA activity and ionic conductivity of the cell decreased too; however, the fixed stoichiometry performance was better than the flow rate method on the whole. This outcome showed that under the same conditions, the fixed stoichiometry mode was better for stability and improved cell performance.

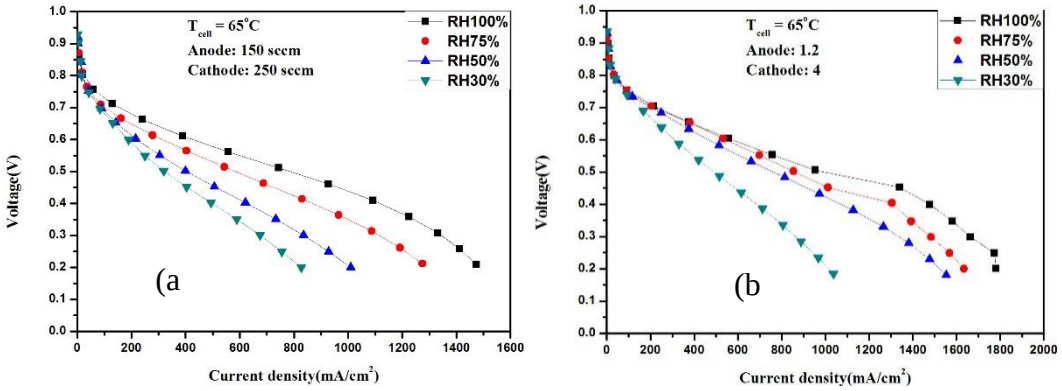

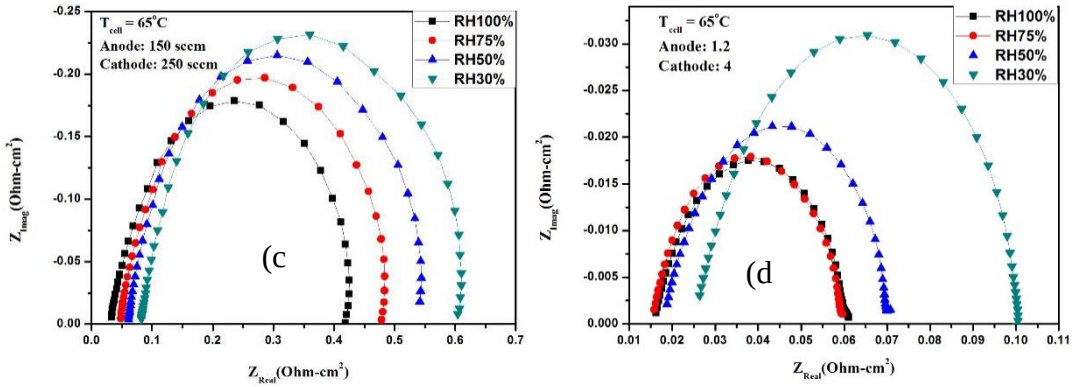

Figure 1. Polarization and impedance curves of different gas supply modes and humidities at 65℃. (a) & (c) Anode: 150 sccm, Cathode: 250 sccm; (b) & (d) Anode: 1.2 stoichiometry, Cathode: 4 stoichiometry

3.1.2 Performance comparison at 80℃

The Nafion®-HP developed by DuPont can operate under high temperature and low humidity. Therefore, the next step is to study the performance of a cell at 80℃ [41]. Figure 2a and c shows the polarization curve and impedance curve of the cell with a fixed flow rate (150 ml/min for the anode and 250 ml/min for the cathode). The cell's performance was 763.12 mA/cm^2 at 100% RH and 0.6 V and 300.54 mA/cm^2 at 50% RH, which was a decrease of 60%. When the relative humidity decreased, the impedance of the cell increased considerably. When the temperature increased, the humidity inside the cell decreased rapidly, which led to decreased MEA activity and ionic conductivity. Figure 2b and d shows the polarization and impedance curves with a fixed stoichiometry (anode: 1.2 times/cathode: 4 times). The cell's performance was 655.93 mA/cm^2 at 100% RH and 0.6 V and 327.63 mA/cm^2 at 50% RH, which was a decrease of 50%. The impedance of the cell did not increase significantly at 75% RH, but increased obviously when the humidity dropped to 50% RH. The water retention of Nafion®-HP decreased rapidly with increased temperature, so the impedance increased rapidly. Figure 2 shows that whether flow or fixed stoichiometry, a decrease of relative humidity significantly decreases and increases the performance and the impedance of the cell, respectively. This outcome was due to an ohmic polarization and a decrease of ionic conductivity in the cell with a decrease of humidity [40, 42]. However, in general, the performance of the cell was much better when the fixed stoichiometry was used instead of flow rate.

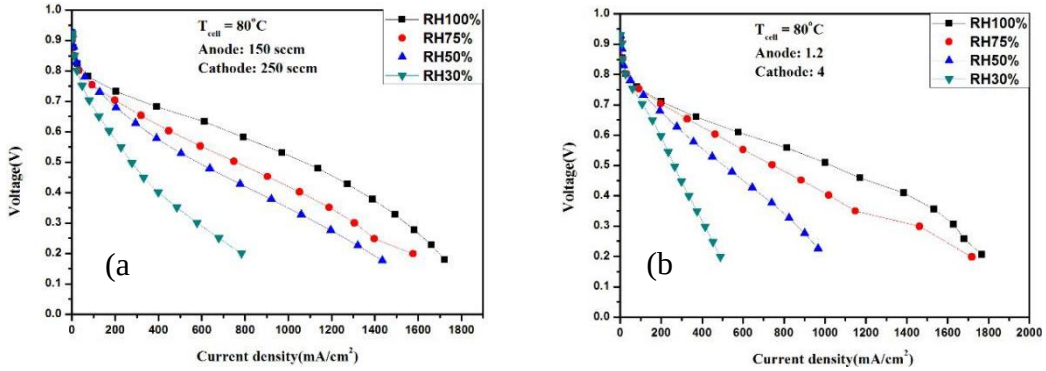

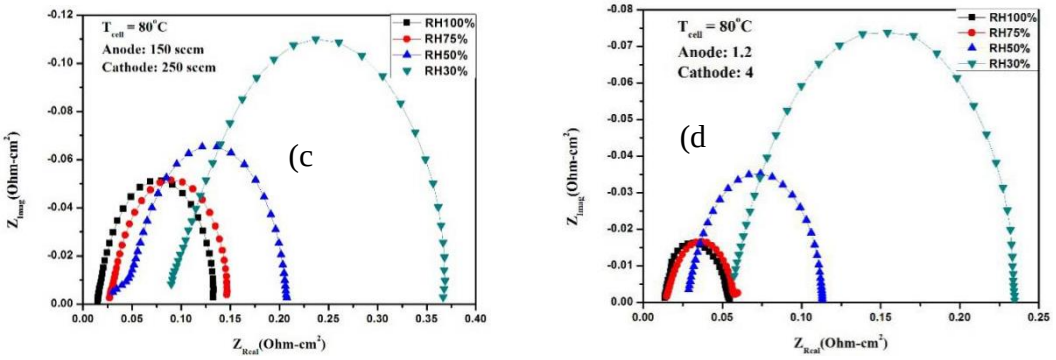

Figure 2. Polarization and impedance curves of different gas flow modes and humidities at 80℃. (a) & (c) Anode: 150 sccm, Cathode: 250 sccm; (b) & (d) Anode: 1.2 stoichiometry, Cathode: 4 stoichiometry

3.1.3 Performance comparison at 85℃

In traffic vehicles, the working temperature of the cells can be as high as 85℃. Therefore, the performance tests of different humidities at 85℃ are carried out to verify whether the Nafion®-HP can maintain its performance. Figure 3a and c shows the polarization curve and impedance curve of the cell at a fixed flow rate (150 ml/min for the anode and 250 ml/min for the cathode). The cell's performance was 738.99 mA/cm^2 at 100% RH and 0.6 V and 343.11 mA/cm^2 at 50% RH. Figure 3b and d shows the polarization curve and impedance curve of a fixed stoichiometry (anode: 1.2 times and cathode: 4 times). The cell's performance was 767.53 mA/cm^2 at 100% RH and 0.6 V and 273.82 mA/cm^2 at 50% RH. Whether flow rate or fixed stoichiometry, the performance of the cell decreased greatly when compared with trials in a fully humid environment; thus, the cell did not meet the performance requirements at high temperature and low humidity. Therefore, it is necessary to improve the membrane material.

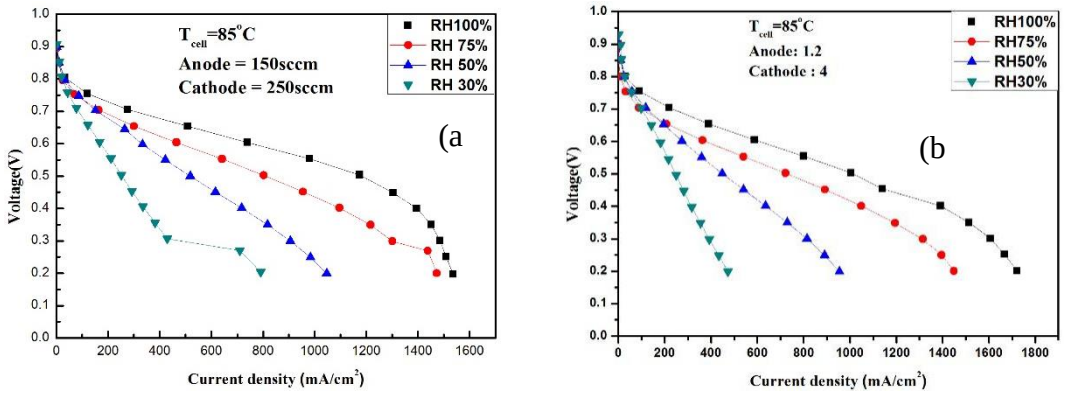

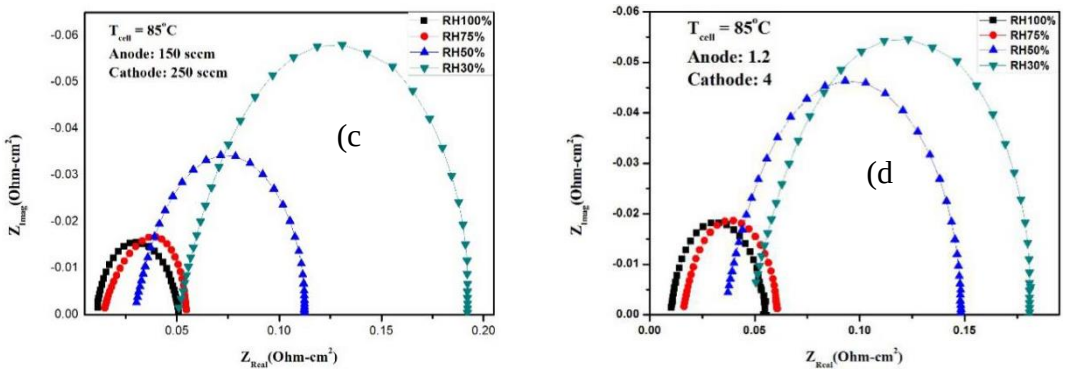

Figure 3. Polarization and impedance curves of different gas flow modes and humidities at 85℃. (a) & (c) Anode: 150 sccm, Cathode: 250 sccm; (b) & (d) Anode: 1.2 stoichiometry, Cathode: 4 stoichiometry

Table 1. Performance comparison of the different gas flow rates, stoichiometries, humidities and temperatures

Flow rate/fixed stoichiometry	150/250 sccm	150/250 sccm	150/250 sccm	1.2/4	1.2/4	1.2/4
temperature	65℃	80℃	85℃	65℃	80℃	85℃
100% RH and 0.6 V	473.5 mA/cm^2	763.12 mA/cm^2	738.99 mA/cm^2	559.12 mA/cm^2	655.93 mA/cm^2	767.53 mA/cm^2
50% RH and 0.6 V	205.8 mA/cm^2	300.54 mA/cm^2	343.11 mA/cm^2	512.02 mA/cm^2	327.63 mA/cm^2	273.82 mA/cm^2
Decline rate	57%	61%	54%	8.4%	50%	64%

Table 1 shows that when the cell is in 100% RH, the flow rate and fixed stoichiometry have their own advantages and disadvantages; however, when the relative humidity is reduced to 50% RH, the performance of the cell is better under the fixed stoichiometry. At present, the research on fuel cell gas supply mainly focuses on the best performance or economic analysis under different stoichiometries [43-45], and a comparative study of fixed stoichiometry and flow rate is less common; thus, this part is one of the innovative points of this paper.

3.2. Changes of ECSA at different temperatures

Cyclic voltammetry (CV) can be used to examine the ECSA [19] of the catalyst. A basic analysis and measurement system was set up with a cell testing machine. Hydrogen (H_2) and nitrogen (N_2) were introduced into the anode and cathode, respectively, and different potentials were applied to observe the area of the hydrogen adsorption peak and desorption peak. Figure 4 shows the CV curves of different cell temperatures at 100% RH. The cell had the best hydrogen adsorption peak and thus, the maximum area at 80℃ , which indicated that the cell has the best performance at 80℃.

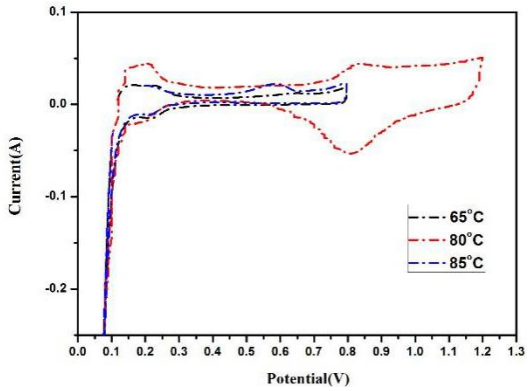

Figure 4. CV curves at different temperatures (65℃, 80℃, 85℃) and 100% RH

3.3. Change of cell performance under different humidities and temperatures by adding SiO_2 to the catalyst layer

Chi-Young Jung [8] and coworkers found that adding SiO_2 to the catalyst layer improved the performance of the cell, but their research focused on the difference of the cell performance by adding SiO_2 of different sizes to the catalyst. Huagen Liang [9] and coworkers added a hydrophilic organic polymer and SiO_2 to a MEA, and successfully prepared a new type of self-humidifying MEA, which exhibited good self-humidifying performance under low humidity conditions. Yilser Devrim [43] and coworkers added SiO_2 in organic solvents and sprayed it on a MEA and found that the acid resistance and ionic conductivity of the MEA could be improved. V. Senthil Velan [46] and coworkers found that when SiO_2 was added to the anode, the performance of the cell increased and the impedance value decreased. In contrast, when SiO_2 was added to the cathode, the ECSA of the cell decreased and the hydrophilicity of the anode increased under a condition of low humidification (50% RH), which was helpful for the stable operation of the fuel cell. Taking into account the water-retention property of SiO_2 [8, 9, 47], the research direction of this part is to add 5 wt% SiO_2 into the MEA with a catalyst content of 0.2/0.4 mg/cm^2 (fixed stoichiometry: 1.2/4) for the anode/cathode to explore whether the cell can achieve good performance stability under high-temperature and low-humidity conditions.

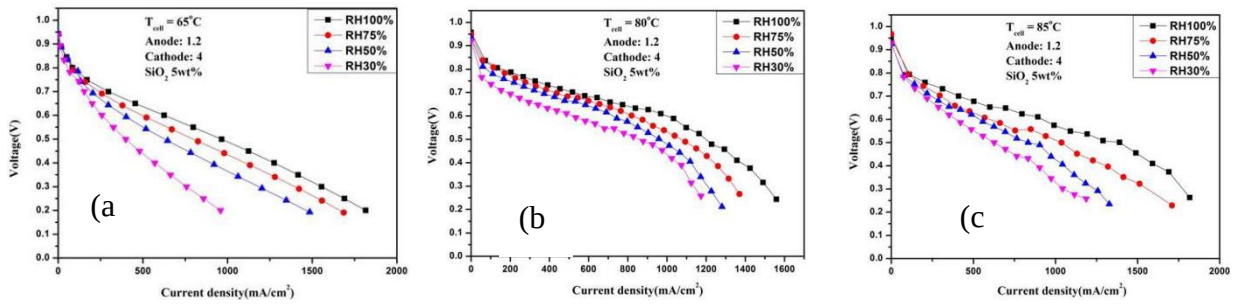

Figure 5. Polarization curves of the catalyst layer with 5 wt% SiO_2 under different humidities and temperatures. Anode: 1.2 stoichiometry, Cathode: 4 stoichiometry

Figure 5a shows the current density is 625.63 mA/cm^2 at 0.6 V under 100% RH and 518.39 mA/cm^2 at 50% RH, which is a decrease of 17%. The water generated by the electrochemical reaction of the cell itself was preserved by adding SiO_2, which improved the water content in the cell; thus, its performance was better than without SiO_2. Figure 5b shows that the performance with 0.6 V was 967.99 mA/cm^2 at 80℃ and 100% RH, while the performance of 50% RH was 632.81 mA/cm^2, which was a decrease of 35%. Compared with a 50% decrease from a catalyst layer without added SiO_2 and under the same working conditions, the decreased performance was greatly reduced. It was found that at low relative humidity, the addition of SiO_2 in the catalyst layer moderately regulated the moisture covering the catalyst surface and improved the performance and stability of the cell. Figure 5c shows a performance of 991.02 mA/cm^2 at 85℃, 100% RH and 0.6 V, which was consistent with the trend of increasing current density when temperature increases. However, the performance at 50% RH was 557.74 mA/cm^2, and the difference of performance between partial humidification and full humidification was 44%. In low humidity, the dehydration of the cell was serious due to the increase of temperature, and the performance of the MEA was greatly declined. Su [48] and coworkers added 10 wt% SiO_2 to a catalyst layer to maintain performance stability at 28% RH. After 120 h of accelerated aging, the decrease in performance was only approximately 10%. However, the operating temperature of this research was 50℃ and found that with the increase of temperature, the performance of the cell decreased rapidly, which was not in line with the actual operating conditions of most fuel cells.

Table 2 shows that under the same working environment, adding 5 wt% SiO_2 can greatly improve the performance of the cell; when the relative humidity drops to 50% RH, adding 5 wt% SiO_2 can reduce the decrease of the cell performance, which indicates that adding SiO_2 can help the cell maintain its performance in a low-humidity environment. The change of humidity had little effect on the performance at low temperature, because low temperature reduces evaporation and was conducive to moisture retention.

Table 2. Performance comparison of catalyst layers with and without SiO_2

SiO_2	No	No	No	5 wt% SiO_2	5 wt% SiO_2	5 wt% SiO_2
		80℃	85℃	65℃		
temperature	65℃	655.93	767.53	625.63	80℃	85℃
100% RH and 0.6 V	559.12 mA/cm^2	mA/cm^2	mA/cm^2	mA/cm^2	967.99 mA/cm^2	991.02 mA/cm^2
50% RH and 0.6 V	512.02 mA/cm^2	327.63	273.82	518.39	632.81 mA/cm^2	557.74 mA/cm^2
Decline rate	8.4%	mA/cm^2	mA/cm^2	mA/cm^2	35%	44%
		50%	64%	17%		

3.4 Expanding the MEA area to 25 cm^2

Research on cell performance under high-temperature and low-humidity conditions has always been a hot topic. Yan Yin and coworkers [11] found a novel Pt-C/Fe-N-S-C cathode dual catalyst layer (CDCL), which was prepared using a catalyst sprayed membrane method. However, the performance was not very stable and seriously deteriorated at high potential (0.7 V). Beom-Soo Koh and coworkers [12] report a nanosized dense-structure (NSDS) layer coated onto a conventional catalyst layer, which

formed a dual-layered electrode architecture that was favorable in promoting the self-humidification process. At 0.6 V under 0% RH, the current density of MEA fabricated by this method was three times higher than that of a traditional MEA. Sanying Hou and coworkers [49] prepared a MEA with a Pt/SnO_2-SiO_2/C anode catalyst and achieved excellent low-humidity performance at 65℃. The improvement of performance was attributed to the increased wettability of SnO_2 and SiO_2 in the cell and the increased platinum activity of SnO_2. Rong-Hsin Huang and coworkers [50] proposed using a sputtering deposition to add hygroscopic zinc oxide (ZnO) nanoparticles to an anodic catalyst layer as a water adsorbent. The MEA with 0.45 wt% ZnO in the anode catalyst layer revealed the best performance at anode humidifier temperatures of 45℃ and 65℃, with power densities 43.91% and 25.80% higher than those without ZnO, respectively.

To meet the needs of commercial applications, the reaction area of MEA was expanded to 25 cm^2, and the stoichiometry was fixed at 1.2 and 4. Figure 6 shows the performance curve at different temperatures and relative humidities. Compared with 5 cm^2, it was found that the cell ran smoothly with an increase of MEA area, and the performance did not fluctuate greatly. This showed that a MEA made by CCM technology had strong stability and the overall design and assembly of the cell was reasonable.

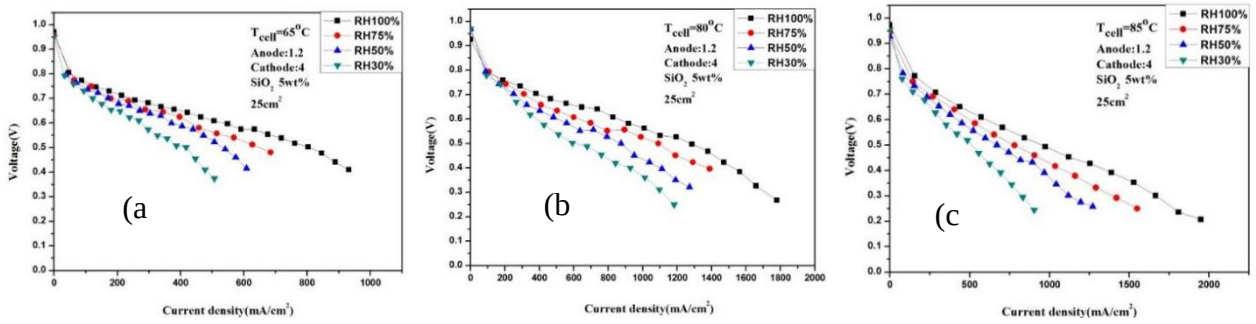

Figure 6. Polarization curves at different temperatures and relative humidities after adding 5 wt% SiO_2 to the catalyst layer (25 cm^2). Anode: 1.2 stoichiometry, Cathode: 4 stoichiometry

Table 3. Performance changes of different areas under different humidities

area	5 cm^2	5 cm^2	5 cm^2	25 cm^2	25 cm^2	25 cm^2
		80℃	85℃	65℃		
temperature	65℃	967.99	991.02	548.46	80℃	85℃
100% RH and 0.6 V	625.63 mA/cm^2	mA/cm^2	mA/cm^2	mA/cm^2	826.36 mA/cm^2	705.60 mA/cm^2
50% RH and 0.6 V	518.39 mA/cm^2	632.81	557.74	428.49	558.06 mA/cm^2	451.20 mA/cm^2
Decline rate	17%	mA/cm^2	mA/cm^2	mA/cm^2	32%	36%
		35%	44%	21%		

Table 3 compares the performance of MEA with an area of 5 cm^2 and 25 cm^2. The cell performance decreased slightly with the increase of MEA area, because gas diffusion and water management were more difficult with the increase of MEA area. However, it was also found that the performance gap between 100% RH and 50% RH decreased to less than 36% with the increase of area, which indicated that the large area MEA operated well in a low-humidity environment. With a

decrease of relative humidity, the performance of the cell also decreased, but regardless of the MEA size, the decrease range was not significantly different, which indicated that the performance of the cell remained stable when the area was enlarged.

3.5 Effect of a dynamic load on cell performance aging during long-term cycling

In this paper, the performance fluctuation of a cell under long working hours was analyzed according to actual working conditions. Referring to relevant studies [51,52,53,54], it was found that the operating temperature of commercial fuel cells was generally below 70℃, because the power system with a smaller volume had less energy consumption. Higher working temperature increased the complexity and volume of insulation equipment, increased the energy consumption of the whole system, and reduced the life of the film. It was also found that temperature changes within a certain range had little effect on cell performance [55]. On the other hand, water management has always been a difficult problem for fuel cells. Reasonable water management will improve the performance of fuel cells, but lack of water management will lead to performance degradation [56, 57, 58]. Relevant studies found that higher temperature reduced the water content in the cell and resulted in decreased conductivity of the membrane [57, 58]. With an increase of temperature, the evaporation rate of water will also increase. When the temperature reaches the critical value of evaporating water exceeding the water output of the fuel cell reaction, the membrane will begin to dry [59, 60, 61, 62] and decreases the performance of the cell. It can be seen from the previous experiments that the cell performance at 65℃ was not much different or even slightly better than at 80℃ and 85℃ at 50% RH. An increased evaporation and decreased membrane wettability led to no expected improvement in cell performance.

To investigate the aging of a small area (5 cm^2) PEMFC under high temperature and low humidity, dynamic high frequency load was used to carry out aging experiments to understand the actual aging situation of the MEA in a PEMFC. Through I-V performance curves, ECSA, AC impedance and the trend of cell performance changes, the key factors that led to MEA aging were studied. The experimental method was cyclic voltammetry with a voltage continuously circulated between 0.6 V and 0.8 V and the anode and cathode introduced to hydrogen and air (1.2 and 4), respectively. The cell was operated under full and partial humidification and the current density and maximum power density are compared at 0.6 V.

3.5.1 Dynamic load during long-term cycling under full humidification

Juhyuk Choi and Bin Li [35, 37] found that the performance degradation rate of cells under long-term dynamic load were reduced by using a new catalyst preparation technology, but it was not much different from this paper. It was found that the main reason for the deterioration of cell performance was the degradation or aggregation of catalysts. Therefore, the technology used in the above papers was mainly to improve the structure or particle size of catalysts.

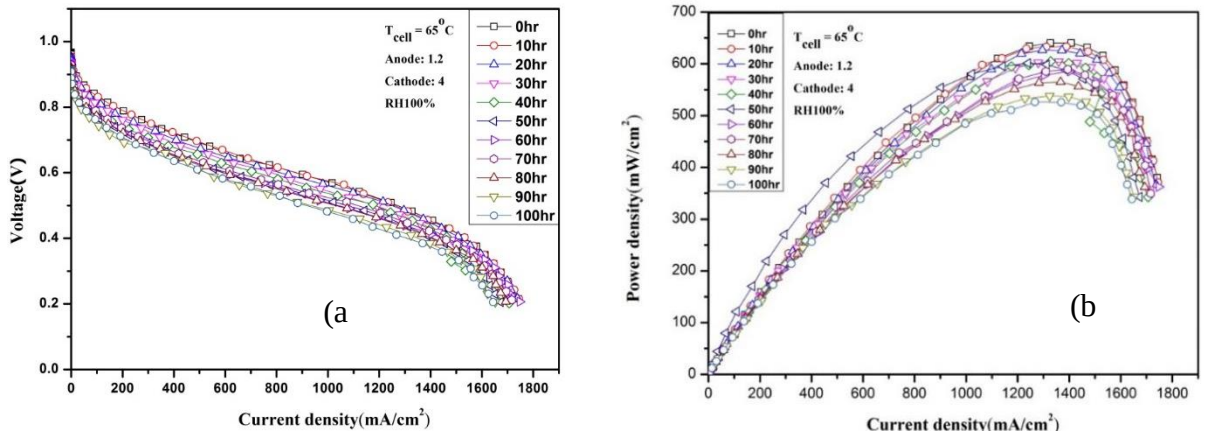

Figure 7. Polarization curves and power density curves of 100-h cyclic dynamic load accelerated aging under full humidification (65℃, 50% RH). Anode: 1.2 stoichiometry, Cathode: 4 stoichiometry

Figure 7 shows a slight decline on fuel cell aging after 60,000 cycles (100 h) under cyclic dynamic load (6 sec/cycle) in full humidity. The parameters of cell performance decline are shown in Table 4. At 0.6 V, the current density at the beginning (0 h) was 856.56 mA/cm^2 and the maximum power density was 640.25 mW/cm^2. After 30 h of cyclic dynamic load, the decrease of current density was 5.11% and the decrease of maximum power density was 6.69%. After 100 h of cyclic dynamic load, the current density (0.6 V) was 623.94 mA/cm^2 and compared with 0 h, the decrease was 27.2%. The maximum power density decreased from 640.25 mW/cm^2 at 0 h to 526.10 mW/cm^2 at 100 h (decreased 17.8%), which was a significant aging in performance. The decline factor was the decrease of ECSA (Pt). The aging of catalyst will be analyzed in detail by cyclic voltammetry (CV).

Table 4. Aging data of 0-100 h (60,000 cycles) with a dynamic load under full humidity

Time	OCV (V)	Maximum power density (mW/cm^2)	Decrease of maximum power density	ECSA (m^2/g_{Pt})	Decrease of ECSA	Current density of 0.6 V (mA/cm^2)	Decrease of current density
0 h	0.967	640.25	_	24.79	_	856.56	_
10 h	0.954	633.31	1.08%	_	_	848.88	0.9%
20 h	0.952	626.25	2.19%	_	_	846.43	1.18%
30 h	0.936	597.43	6.69%	_	_	812.79	5.11%
40 h	0.903	601.94	5.98%	_	_	805.47	5.96%
50 h	0.91	601.38	6.07%	19.34	21.9%	776.59	9.34%
60 h	0.91	585.73	8.52%	_	_	745.18	13%
70 h	0.90	585.39	8.57%	_	_	739.99	13.6%
80 h	0.919	564.95	11.8%	_	_	700.06	18.3%
90 h	0.914	536.80	16.2%	_	_	655.02	23.5%
100 h	0.887	526.10	17.8%	16.53	33.3%	623.94	27.2%

3.5.2 Dynamic load during long-term cycling under partial humidity

Figure 8 is the aging performance curve of the cell under a partial humidity cyclic dynamic load of 100 h (6 sec/cycle). Detailed data about the performance decline can be found in Table 5. After 30 h, the decrease of current density was 8.35% and the decrease of maximum power density was

8.19%. After 60 h, the decrease of current density and maximum power density were 40.1% and 28.4%, respectively. The data showed that the decreased performance of MEA produced by CCM technology was more serious under partial humidity than full humidity. Under a condition of partial humidity, the gas flow in the cell reduced the wettability of the MEA, which resulted in the instability of the cell performance.

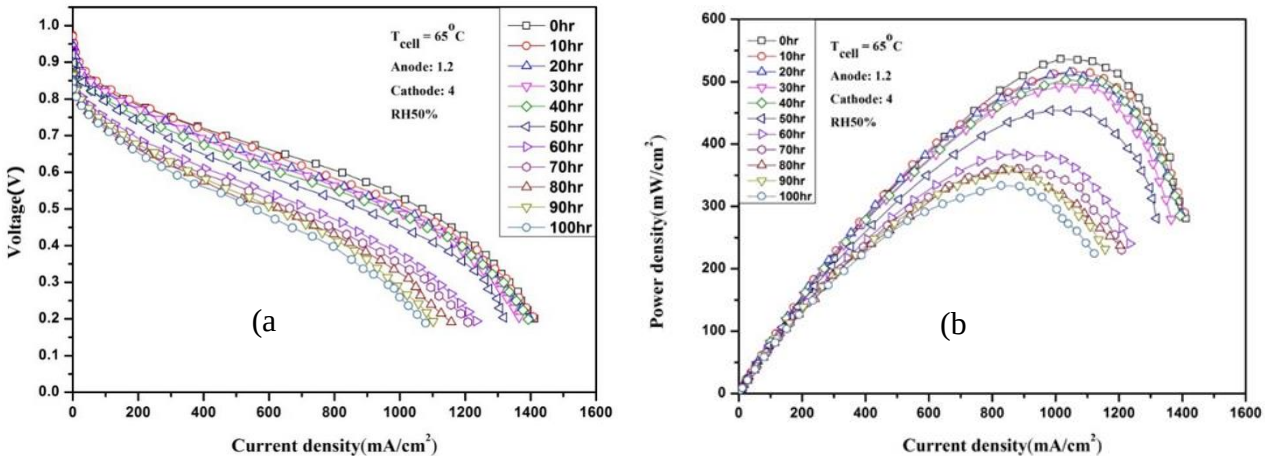

Figure 8 Polarization curves and power density curves of 100-h dynamic load accelerated aging under partial humidity (65℃, 50% RH). Anode: 1.2 stoichiometry, Cathode: 4 stoichiometry

Table 5. Aging data of 0-100 h (60000 cycles) with a dynamic load under partial humidity

Time	OCV (V)	Maximum power density (mW/cm^2)	Decrease of maximum power density	ECSA (m^2/g_{Pt})	Decrease of ECSA	Current density of 0.6 V (mA/cm^2)	Decrease of current density
0 h	0.952	536.25	_	18.76	_	804.20	_
10 h	0.973	515.88	3.79%	_	_	774.52	3.69%
20 h	0.946	514.44	4.07%	_	_	767.44	4.57%
30 h	0.935	492.35	8.19%	_	_	737.08	8.35%
40 h	0.903	502.69	6.26%	_	_	732.14	8.96%
50 h	0.905	453.96	15.3%	11.78	37.2%	570.23	29.1%
60 h	0.872	384.09	28.4%	_	_	481.55	40.1%
70 h	0.839	360.59	32.8%	_	_	469.37	41.6%
80 h	0.823	357.51	33.3%	_	_	417.74	48.1%
90 h	0.828	350.19	34.7%	_	_	402.12	50%
100 h	0.834	333.52	37.8%	8.38	55.3%	387.43	51.8%

3.6 Diagnostic analysis of cell performance aging

Based on the performance change of the cell after long-term cycling of a dynamic load in section 3.5, the causes of the decline of cell performance and MEA aging were analyzed by measuring the changes of catalyst ECSA, AC impedance and OCV under different working conditions.

3.6.1 Effect of a dynamic load on the ECSA during long-term cycling

The ECSA on the catalyst electrode was examined by cyclic voltammetry. The reverse potential scanning of CV was to observe the phenomenon of hydrogen adsorption and desorption. The scanning rate set by the experimental operation was relatively fast. Figure 9 shows CV curves of 100 h of cyclic dynamic load. After cyclic dynamic load was completed, the causes were analyzed according to the results of catalyst aging. Cyclic voltammetry can observe the electrochemical phenomena by using the current value corresponding with the scanning voltage to distinguish the decline of catalyst activity by observing the characteristics of CV curves. The largest ECSA was found at 0 h after the activation of MEA, and the ECSA decreased gradually over time.

The ECSA was calculated by using the hydrogen adsorption peak and the capacitance of the electric double layer. The change of ECSA after a 100-h cyclic dynamic load was studied under 100% RH and 50% RH. Figure 9a shows that the ECSA was 24.79 (m^2/g_{Pt}) under full humidity and Figure 9b shows the ECSA was 18.76 (m^2/g_{Pt}) under partial humidity. It was found that the difference of cell performance under different humidities was due to the difference of the ECSA caused by the different concentration of active catalyst on the MEA, which indicated that the aging of the MEA caused by cyclic dynamic loading was closely related to the decreased active area of the MEA.

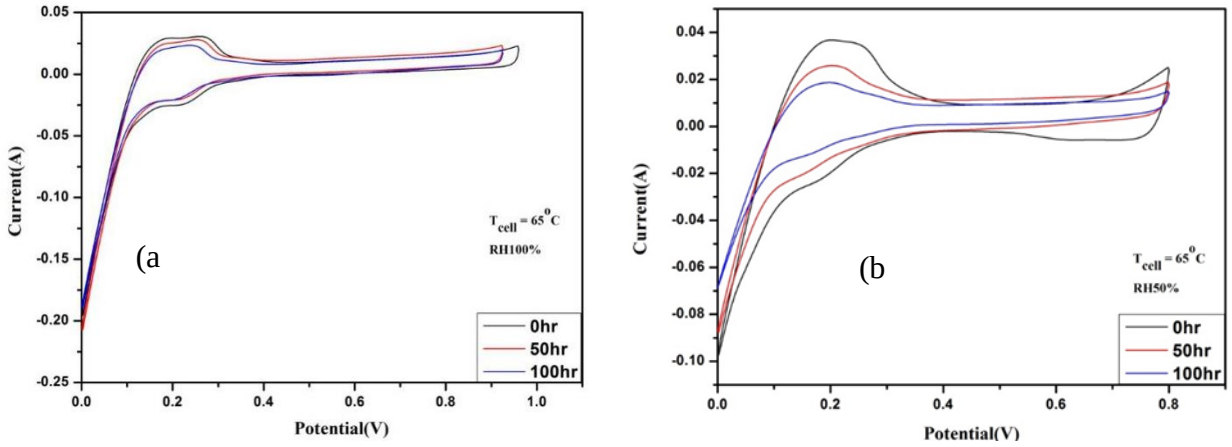

Figure 9 Effects of cyclic dynamic load on the ECSA under full and partial humidity (65℃)

F. Ettingshausen and coworkers [63] found that under the start/stop conditions in automotive operation, there was pronounced platinum dissolution accompanied by the formation of large platinum precipitations in the membrane. The corrosion of carbon plates was also observed, but no significant reduction in porosity and loss of platinum were observed. In contrast, MEA at high constant potential caused serious damage to a 3D cathode structure due to carbon corrosion. Josef C. Meier and coworkers [64] found four different degradation pathways where one single Pt/Vulcan aggregate was clearly observed and inhomogeneous degradation behavior for different catalyst locations was shown; the importance of particle size, as well as the catalyst pretreatment, on the degradation mechanism was emphasized. Takeshi Yoda and coworkers [65] found that high potential and/or high temperature led to

a significant decrease in the ECSA of a cell, which also proved the rationality of the experimental parameters in this paper.

The CV curves scanned by cyclic voltammetry showed that the current between 0.4 V and 0.8 V was not much different, which indicated that the corrosion of the carbon plate, the carrier of the catalyst, did not increase continuously. This result indicated that the main reason of cell aging and performance decline caused by cyclic dynamic loading was the reduction of ECSA of the catalyst. However, the reduction of ECSA of the catalyst was not caused by carbon plate corrosion, but by the rapid switching of the load, which resulted in the aggregation of the catalyst. It was found from the measurement results that at 50% RH, the degree of decline of the ECSA was more than 100% RH. The decrease of the ECSA at 50% RH was 55.3% after 100 h, while that at 100% RH was 33.3%. The reason was the moisture content of the MEA was too low, which led to decreased wettability and cell performance.

3.6.2 Effect of dynamic load on AC impedance during long-term cycling

Figure 10 shows the effect of voltage on the AC impedance in an accelerated aging test of the cell at different cycle times. The curves were quadratic curves in complex coordinates, and the first intersection point of the real axis was the resistance obtained by high frequency AC scanning. According to the equivalent circuit theory, its impedance is the total impedance (R_b), which ignores the capacitance effect. It was regarded as the MEA impedance under the same operating conditions and cell. The difference between the two intersection points of the curve to the real axis is the charge-transfer impedance (R_{ct}) caused by low frequency scanning, which can be regarded as the catalyst layer impedance under the same operating conditions and cell. At 50% RH, the translation of the curves along the X-axis and the ohmic loss were particularly serious.

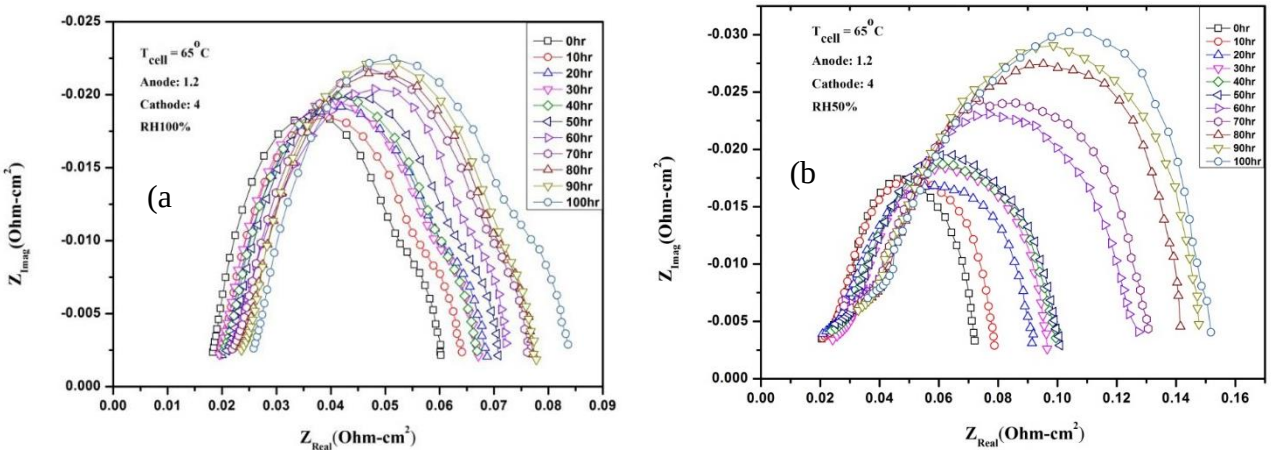

Figure 10 Effects of cyclic dynamic load on AC impedance under full and partial humidity. Anode: 1.2 stoichiometry, Cathode: 4 stoichiometry, 65°C, 100% RH and 50% RH

3.6.3 Effect of dynamic load on ohmic impedance and Rc impedance during long-term cycling

Figure 11 shows the ohmic impedance(R_Ω) and contact impedance (R_c) of a cyclic dynamic load under different levels of humidity. The performance under full humidity was much better than

that under partial humidity. The impedance (R_b) obtained from AC impedance (EIS) is only the intrinsic resistance of cell materials, which includes electrolytes, electrodes, current collectors and the resistance of the lead wire itself. The total ohmic impedance (R_Ω) obtained from the voltage-current curve fitting includes not only the intrinsic resistance of the cell, but also the structural resistance and the contact resistance between the two phases. Therefore, the ohmic impedance obtained from the voltage-current curve is larger than that from the AC impedance (Table6), and the difference between the two is the contact impedance of the cell.

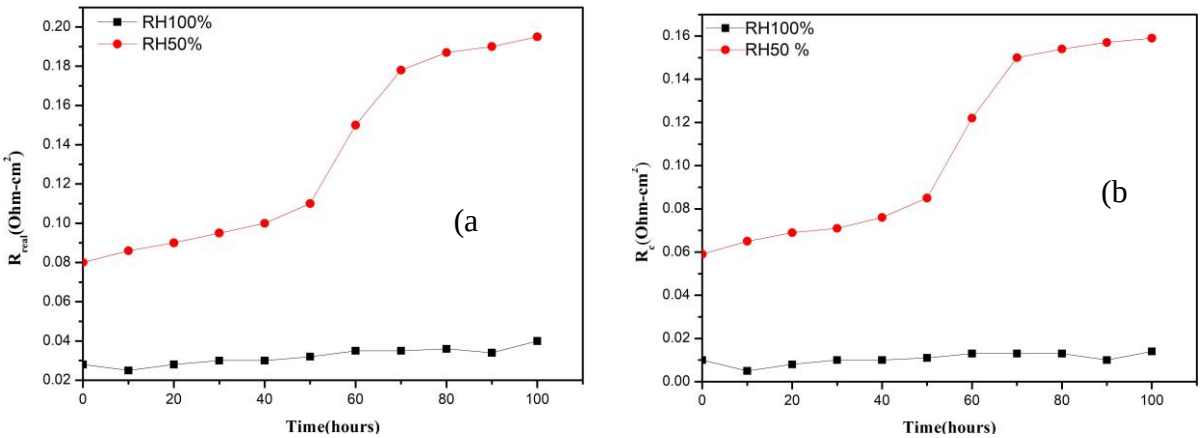

Figure 11. Cyclic dynamic load curves of ohmic impedance and R_c impedance under different humidities (100% RH and 50% RH)

Table 6. R_Ω, R_c,R_{ct} and R_b analysis data of 0-100 h (60,000 cycles) under different humidities

	100% RH R_Ω (Ohm-cm^2)	50% RH R_Ω (Ohm-cm^2)	100% RH R_c (Ohm-cm^2)	50% RH R_c (Ohm-cm^2)	100% RH R_{ct} (Ohm-cm^2)	50% RH R_{ct} (Ohm-cm^2)	100% RH R_b (Ohm-cm^2)	50% RH R_b (Ohm-cm^2)
0 h	0.028	0.08	0.01	0.059	0.042	0.052	0.018	0.021
10 h	0.025	0.086	0.005	0.065	0.044	0.058	0.02	0.021
20 h	0.028	0.09	0.008	0.069	0.049	0.071	0.02	0.021
30 h	0.03	0.095	0.01	0.071	0.048	0.072	0.02	0.024
40 h	0.03	0.1	0.01	0.076	0.047	0.076	0.02	0.024
50 h	0.032	0.11	0.011	0.085	0.05	0.076	0.021	0.025
60 h	0.035	0.15	0.013	0.122	0.05	0.099	0.022	0.028
70 h	0.035	0.178	0.013	0.15	0.054	0.103	0.022	0.028
80 h	0.036	0.187	0.013	0.154	0.054	0.109	0.023	0.033
90 h	0.034	0.19	0.01	0.157	0.054	0.115	0.024	0.033
100 h	0.04	0.195	0.014	0.159	0.058	0.116	0.026	0.036

Table 6 and figure 11a shows that the ohmic impedance (R_Ω) of the cell increased rapidly at 50% RH. The saturation of water content in the MEA affected the ionic conductivity of the proton exchange membrane (PEM). When the water content in the membrane was reduced, the impedance of ion conduction increased. At 100% RH, the R_Ω did not significantly increase during the accelerated aging test, but the semicircle curves of charge-transfer impedance increased with an increased cycle number, which indicated that the catalyst or proton conductor in the catalyst layer gradually declined during the accelerated aging test. The increased charge-transfer impedance indicated the aging of the

catalyst layer, which coincided with the loss of the ECSA mentioned above and caused a decreased OCV.

According to the test results of AC impedance, ohmic impedance and R_c impedance, the R_c value decreased sharply when the current increased, so the lower R_c value meant relatively higher cell performance. Table 6 shows four impedances analysis data of 0-100 h (60,000 cycles) under different humidities. At 50% RH, the R_c value from 0-50 h was between 0.06-0.085 Ω-cm^2 and from 60-100 h, the R_c value was between 0.12-0.16 Ω-cm^2, which indicated that the performance significantly declined after 60 h. At 100% RH, the increase of $R_Ω$, R_c, R_{ct} and R_b are much less than 50% RH, and the change trend of the four are similar. Table 6 shows $R_Ω$, R_c, R_{ct} and R_b of the cell increase with the increase of the cycle load time, which indicates that the performance degradation of the cell is multifaceted.

3.6.4 Effect of dynamic load on OCV during long-term cycling

Figure 12 shows the effect of cyclic dynamic load on the OCV of the cell under full and partial humidity. The OCV of the cell was stabilized for 10 min before the cyclic dynamic load was applied. Figure 12a shows that the OCV decreases slightly during 100 h of operation under full humidity. It was inferred that after 60,000 cycles of cyclic dynamic load, the performance of the cell would decline slightly but still run steadily.

Figure 12b shows that although the OCV is high from 0-30 h under partial humidity, the OCV significantly decreases after 50 h, indicating that the OCV decrease under different humidities is consistent with the decline in performance and the ECSA.

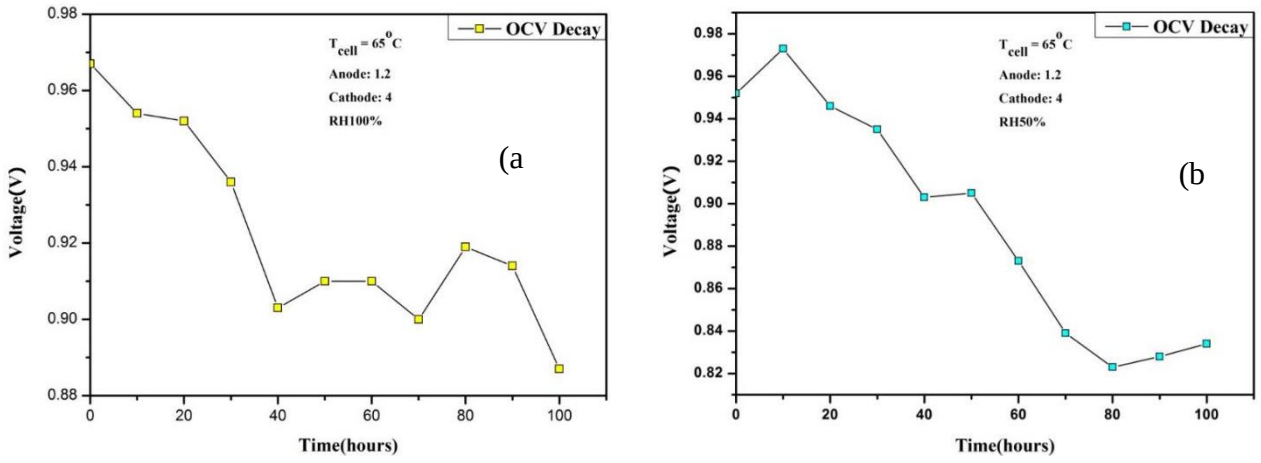

Figure 12. OCV decline curves with full and partial humidity under cyclic dynamic load. Anode: 1.2 stoichiometry, Cathode: 4 stoichiometry, 65°C, 100% RH and 50% RH

4. CONCLUSION

In this paper, a Nafion®-HP membrane was used as the base of a MEA, and isopropanol was used as a solvent instead of ethanol. CCM spraying technology was used to spray the catalyst onto the

surface of the MEA. By adding water-retaining materials in the MEA for the aging test, the following conclusions were obtained.

Previous experiments showed that the performance and stability of the cell were better when the gas was fed with a fixed stoichiometry method at high humidity (100% RH) or low humidity (50% RH) than when fed with a flow rate mode. Through the impedance measurement of the cell, it was found that the increase of ohmic impedance and polarization impedance of the cell was small when the gas had a fixed stoichiometry, which indicated that the cell had good water retention under the same conditions.

Based on the hydrophilicity of SiO_2, 5 wt% SiO_2 was added to the catalyst layer. It was found that the addition of SiO_2 improved the water retention and the performance of the cell at low relative humidity, which proved that SiO_2 helped the cell work in a low-humidity environment.

Expanding the MEA area from 5 cm^2 to 25 cm^2 showed that the performance of the cell fluctuated within 20%, which indicated that the MEA made by CCM technology met the performance requirements.

Cyclic voltammetry (CV) was used to test cell aging. After 100 h (60,000 cycles) of high frequency cyclic dynamic load, it was found that the electrochemically active surface area (ECSA) of the Pt catalyst gradually decreased over time; however, the catalyst carrier (carbon plate) did not seriously corrode, which indicated that the reason for the decrease of ECSA was the aggregation or oxidation of the catalyst itself.

In the accelerated aging test under full and partial humidity, the partial humidity performance decrease was obviously faster than that under full humidity, which indicated that the humidity inside the cell varied greatly with the increase of operating time, and the water content was an important factor that affected the aging of the cell. At the same time, it was found that under partial humidity, the increase of cell impedance was faster and the fluctuation of OCV was larger than those under full humidity due to the decrease of the MEA wettability.

References

1. M. Hu, Z. Li and G. Cao, *Int. J. Electrochem. Sci*., 14 (2019) 651.
2. G. Hu, C. Ji, Y. Xia, Y. Suo, X. Wu and Z. Zhang, *Int. J. Electrochem. Sci*., 14 (2019) 1358.
3. Y. Tian, Z. Lü, X. Guo and P. Wu, *Int. J. Electrochem. Sci*., 14 (2019) 1093.
4. Ahmed DH, Sung H. J, Bae J and Lee DR, *Int. J. Heat Mass Tran*., 51 (2008) 2006.
5. Steiner NY, Mocoteguy P, Candusso D, Hissel D, Hernandez A and Aslanides A, *J. Power Sources*, 183 (2008) 260.
6. W. Dai, H. Wang, X. Yuan, J.J. Martin, D. Yang and J. Qiao, *Int. J. Hydrogen Energy*, 34(2009) 9461.
7. S. Hou, H. Su, H. Zou, D. Dang, H. Song, X. Li and S. Liao, *Int. J. Hydrogen Energy*, 40 (2015) 613.
8. C. Jung, J. Yi and S. Yi, *Energy*, 68 (2014) 794.
9. H. Liang, D. Dang, W. Xiong, H. Song and S. Liao, *J. Power Sources*, 241 (2013) 367.
10. C.W. Roh, J. Choi and H. Lee, *Electrochem. Commun*., 97(2018) 105.
11. Y. Yin, J. Liu, Y. Chang, Y. Zhu, X. Xie, Y. Qin and J. Zhang, *Electrochim. Acta*, 296 (2019) 450.
12. B. Koha, J. Yooa, E. Janga, Vasanth Rajendiran Jothia, C. Jungb and S. Yi, *Electrochem. Commun*.,

93(2018) 76.
13. S. Martin, P.L. Garcia-Ybarra and J.L. Castillo, *Appl Energ*., 205 (2017) 1012.
14. Mulyazmi, W.R.W. Daud, E.H. Majlan and M.I. Rosli, *Int. J. Hydrogen Energy*, 38 (2013) 09.
15. Vincenzo Liso, Samuel Simon Araya and Anders Chrsistian Olesen, *Int. J. Hydrogen Energy*, 41 (2016) 79.
16. Pietro P. Lopes, Dusan Tripkovic and Pedro F.B.D, *J. Electroanal. Chem*., 819 (2018) 123.
17. Nejc Hodnik, Milena Zorko, Barbara Jozinović, Marjan Bele and Goran Dražič, *Electrochem. Commun*., 30 (2013) 75.
18. Laetitia Dubau, Miguel Lopez-Haro, Luis Castanheira, Julien Durst and Marian Chatenet, *Appl. Catal. B-environ*., 142 (2013) 801.
19. S.R. Dhanushkodi, S. Kundu, M.W. Fowler and M.D, *J. Power Sources*, 245 (2014) 35.
20. Milena Zorko, Barbara Jozinović, Marjan Bele, Nejc Hodnik and Miran Gaberšček, *Ultramicroscopy*, 140 (2014) 44.
21. G.R. Mirshekari and C.A, *J. Power Sources*, 396 (2018) 606.
22. Miguel Lopez-Haro, Laetitia Dubau, Laure Guétaz and Pascale Bayle-Guillemaud, *Appl. Catal. B-environ.*, 152 (2014) 300.
23. Nyccolas E. Souza, Jose L. Bott-Neto, Thairo A. Rocha and Gabriel C. da Silva, *Electrochim. Acta*, 265 (2018) 523.
24. P. Dhanasekaran, S. Vinod Selvaganesh, Avanish Shukla, N. Nagaraju and S.D. Bhat, *Electrochim. Acta*, 263 (2018) 596.
25. Napapat Chaisubanan, Witchaya Maniwan and Mali Hunsom, *Energy*, 127 (2017) 454.
26. Chikara Takei, Katsuyoshi Kakinuma, Kazuhito Kawashima and Keisuke Tashiro, *J. Power Sources*, 324 (2016) 729.
27. Y. Park, Katsuyoshi Kakinuma, Makoto Uchida and Hiroyuki Uchida, *Electrochim. Acta*, 123 (2014) 84.
28. L. Dubau, L. Castanheira, G. Berthomé and F. Maillard, *Electrochim Acta*, 110 (2013) 273.
29. L. Wang, Y. Zhou and Miriam H. Rafailovich, *ACS Catal*., 9(2019)1446.
30. L. Wang, Y. Zhou, C. Nam and Miriam H. Rafailovich, *ACS Appl. Energy Mater*., 2(2019)3479.
31. G. Zhang, Q. Li, W. Chen, X. Meng and H. Deng, *Int. J. Hydrogen Energy*, 44(2019)370.
32. T. Wang, Q. Li and H. Yang, *Energy Convers. Manage*., 196(2019)866.
33. Kazuhiko Shinohara, Atsushi Ohma and Akihiro Iiyama, *220th ECS Meeting*, 1103(2011).
34. L. Yin, Q. Li and W. Chen, *Int. J. Hydrogen Energy*, 44(2019)5499.
35. J. Choi, J. Jang and C. Roh, *Appl. Catal. B-environ*., 225(2018)530.
36. W. Li, R. Lin and Y. Yang, *Electrochim. Acta*, 302(2019)241.
37. B. Li, Drew C. Higgins and Q. Xiao, *Appl. Catal. B-environ*., *1*62(2015)133.
38. Bosung Kim, Dowon Cha and Yongchan Kim , *Appl Energ*., 138(2015)143.
39. B.H. Lim, E.H. Majlan, W.R.W. Daud, M.I. Rosli and T. Husaini, *Energy*, 168(2019)338.
40. Pourya Karimi Takalloo, Ehsan Shabahang Nia and Mohsen Ghazikhani, *Energy Convers. Manage*., 114 (2016) 290.
41. Dilek Nur Ozen, Bora Timurkutluk and Kemal Altinisik, *Renew Sust Energ. Rev*., 59 (2016) 1298.
42. Hyo-Yup Kim and Kyoungyoun Kim, *Int. J. Hydrogen Energy*, 41 (2016) 776.
43. S. Li and Bengt Sunden, *Int. J. Hydrogen Energy*, 42 (2016) 323.
44. Torsten Berning, *Int. J. Hydrogen Energy*, 39 (2014) 449.
45. C. Li, S. Wu and W. Yu, *Int. J. Hydrogen Energy*, 39 (2014) 4502.
46. V.Senthil Velan, G.Velayutham and Neha Hebalkar, *Int. J. Hydrogen Energy*, 36 (2011) 14815.
47. Ylser Devrim, Hu seyin Devrim and Inci Eroglu, *Int. J. Hydrogen Energy*, 41 (2016) 44.
48. H. Su, L. Yang, S. Liao and Q. Zeng, *Electrochim. Acta*, 55 (2010) 8894.
49. S. Hou, R. Chen, H. Zou and T. Shu, *Int. J. Hydrogen Energy*, 41(2016)9197.
50. R. Huang, T. Chiu, T. Lin, C. Sun and W. Chao, *J. Power Sources*, 227(2013)229.
51. C. Hsieh, Xuan-Vien Nguyen, F. Weng, T. Kuo, Z. Huang and A. Su, *Int. J. Electrochem. Sci*.,

11(2016)10449.
52. Erni Misran, Nik Suhaimi Mat Hassan and Wan Ramli Wan Daud, *Int. J. Hydrogen Energy*, 38(2013)9395.
53. B. Wang, R. Lin, D. Liu, J. Xu and B. Feng, *Int. J. Hydrogen Energy*, 44(2019)13737.
54. Chrysovalantou Ziogou, Spyros Voutetakis, Simira Papadopoulou and Michael C. Georgiadis, *Comput. Chem. Eng*., 35(2011)1886.
55. S. Xia, R. Lin, X. Cui and J. Shan, *Int. J. Hydrogen Energy*, 41(2016)26.
56. Srinivasan Raman, K.B. Iyeswaria, Sridharakumar Narasimhan and Raghunathan Rengaswamy, *Int. J. Hydrogen Energy*, 42(2017)23799.
57. M. Pérez-Page and V. Pérez-Herranz, *Int. J. Electrochem. Sci*., 6(2011)492.
58. O.S. Ijaodola, Zaki El- Hassan, E. Ogungbemi, F.N. Khatib and Tabbi Wilberforce, *Energy*, 179(2019)246.
59. Q. Yan, H. Toghiani and H. Causey, *J. Power Sources*, 161 (2006) 492.
60. Q. Yan, H. Toghiani and J. Wu, *J. Power Sources*, 158 (2006) 316.
61. M.M. Saleh, T. Okajima, M. Hayase, F. Kitamura and T. Ohsaka, *J. Power Sources*, 164 (2007) 503.
62. L. Wang, A. Husar, T. Zhou and H. Liu, *Int. J. Hydrogen Energy*, 28 (2003) 1263.
63. F. Ettingshausen, J. Kleemann, A. Marcu, G. Toth, H. Fuess and C. Roth, *Fuel Cells*, 2(2011)11.
64. Josef C. Meier, Carolina Galeano, Ioannis Katsounaros and Angel A. Topalov, *ACS Catal*., 2(2012)832.
65. TakeshiYoda, Hiroyuki Uchida and MasahiroWatanabe, *Electrochim. Acta*, 52(2007)19.